Detection of Weak Astronomical Signals with Frequency-Hopping Interference Suppression[☆]

Shengheng Liu[a,b,c], Yimin D. Zhang[b], Tao Shan[a,*]

[a]*School of Information and Electronics, Beijing Institute of Technology, Beijing 100081, China*
[b]*Department of Electrical and Computer Engineering, Temple University, Philadelphia, PA 19122, USA*
[c]*School of Engineering, The University of Edinburgh, Edinburgh EH9 3JL, UK*

Abstract

This paper addresses the detection of weak astronomical signals that are contaminated by strong frequency-hopping (FH) interferers and suffer from missing samples. The problem is considered in the time-frequency domain and we successively suppress artifacts due to missing samples, estimate and remove FH interferers, and detect the weak astronomical signals. More specifically, we first suppress the artifacts due to missing samples by developing a waveform-adaptive time-frequency kernel. The instantaneous spectra of the FH interferers are then estimated using a sparsity-based approach that takes the inherent properties of FH signals into account. Finally, a sparse coherent integrated cubic phase function is applied to effectively detect weak astronomical chirp components over a long integration time. Simulation results are provided to demonstrate the effectiveness of the proposed approach.

Keywords: Time-frequency analysis; kernel design; radio telescope; Bayesian compressive sensing; frequency hopping

---

*Corresponding author.
Email address:* `shantao@bit.edu.cn` (Tao Shan)

Nomenclature

$\jmath$	$\sqrt{-1}$
$\mathbf{F}_d/\mathbf{F}_d^{-1}$	One-dimensional forward/inverse discrete Fourier transform (DFT/IDFT) matrices with respect to (w.r.t.) the d dimension
$\mathbf{F}_{d_1,d_2}$	Two-dimensional DFT w.r.t. the d_1 and d_2 dimensions
$\circ$	Element-wise (Hadamard) product operator
$(\cdot)^{\mathrm{T}}$	Transpose operation
$(\cdot)^*$	Conjugate operation
mod	Modulo operation
$p(\cdot)$	Probability density function (PDF)
$\mathcal{CN}(\cdot)$	Complex Gaussian distribution
$\mathcal{B}(\cdot)$	Bernoulli distribution
$\mathrm{Gamma}(\cdot)$	Gamma distribution
$\mathrm{Beta}(\cdot)$	Beta distribution
$|\cdot|$	Cardinality of a set
$\lfloor\cdot\rfloor$	Floor fucntion

1. Introduction

Radio astronomy is recognized as a vitally important field that explores the universe and broadens the human perspective. As astronomical signals span a broad frequency spectrum, they are interfered by a growing number of terrestrial radio frequency signals from various sources. While a radio telescope array typically performs coherent beamforming for signal enhancement and radio frequency interference (RFI) mitigation, residual RFIs from array sidelobes may often remain above the desired sensitivity level [3]. This problem is compounded with the fact that the desired signal is extremely weak, as inferred by, e.g., the recent discoveries made by the Laser Interferometer Gravitational-Wave Observatory (LIGO) [4]. As such, detection of weak astronomical signals in the presence of strong interference represents one of the main research problems in the radio astronomy field [5]. Astronomical signals typically have time-varying spectra that are characterized by their instantaneous frequencies (IFs). Because the variation of the IFs is primarily due to the Doppler effects from the relative motion between the observed astronomical sources and the telescope array, the IFs typically exhibit a linear frequency modulated (LFM) behavior over a moderate processing time period. For example, the dynamic spectrum of the observed signal from Crab

pulsar precisely follows an LFM characteristic over a time duration of 0.08 s [6].

Some important frequency bands are protected for exclusive radio astronomy use [7]. However, they could be very close to legal high power broadcasting or communication users which, even with well-designed transmitters, may have spurious signals that are leaked into these protected bands with a much higher signal level than the desired radio astronomical signals. The situation becomes much worse when frequency band allocations overlap. For example, the $225 - 328.6$ MHz band is used to provide frequency-hopping (FH) radio communications for tactical air-to-air and air-to-ground-to-air communications [8], while the $322.0 - 328.6$ MHz band is an important spectrum used in several United States and European radio astronomy observations for low-frequency observations of pulsars and flare stars [7–9]. FH signals are commonly used in a wide range of wireless communication systems because of many unique features such as resistance to jamming and multipath fading, as well as low probability of intercept. In this paper, multiple fast FH signals are considered as interferers and thus must be effectively suppressed before desired weak astronomical signals can be detected. Because FH signals are received through terrestrial propagation, they are likely to experience missing observations due to path obstruction and fading. In this case, existing FH parameter estimation methods [10, 11] do not offer desirable performance.

Both LFM and FH signals can be categorized as nonstationary because they exhibit time-varying spectral contents. To analyze such signals, various time-frequency representations (TFRs) have been proposed [12–20]. In particular, the separable kernel TFRs [12, 13] outperform the conventional TFRs in terms of the resolution and energy concentration properties. Nevertheless, in the cases where the desired signal components distribute away from the axes in the time-frequency plane, the separable kernel TFRs cannot achieve adequate energy concentration. Reassignment methods [14, 15] concentrate the energy distribution of these desired signal components towards their centers of gravity, yielding effective sharpening of the TFRs. On this basis, less deformation of the IF profile is achieved with synchrosqueezing methods [16–18], which are variants of the reassignment family. However, since these methods aim to simultaneously localize noise and signal components, the different signal components of interest become difficult to resolve in low signal-to-noise ratio (SNR) conditions. The empirical wavelet transform (EWT) approach [19] adaptively decomposes the signal by constructing a wavelet filter bank with the underlying spectrum information, which relies

3

on robust preprocessing for peak detection to a great extent, and its performance degrades in the low SNR region as well. A modified version of the EWT is presented in [20], where segmentation boundaries are created by exploiting the MUSIC estimation. However, as the spectrum shape is ignored in the boundary estimation process, a sufficiently satisfactory segmentation cannot be obtained. In addition, none of them investigated the robust FH spectrum estimation in the presence of missing samples.

The method developed in this paper achieves robust FH spectrum estimation in the presence of missing data and, as a result, enables effective suppression of the FH interferers for weak astronomical signal detection. Toward this end, a waveform-adaptive time-frequency kernel and the adaptive optimal kernel (AOK) are first applied to mitigate the effect of missing samples, and a Bayesian compressive sensing (BCS) based technique, which takes the inherent characteristic of FH signals into account, is used for FH spectrum estimation. After FH interference removal, the weak LFM astronomical signals are detected and estimated via the coherent integrated cubic phase function (CICPF), which is efficiently implemented by applying the sparse Fourier transform (SFT) [21]. The contributions of this work is threefold: (1) A two-stage kernel design that combines pre-filtering based on the inherent FH signal characteristic and the standard signal-dependent adaptive kernel is proposed to mitigate artifacts due to missing samples and obtain enhanced joint-variable representation of the FH signals; (2) A structure-aware BCS technique is exploited to achieve improved signal spectrum and IF estimations; (3) A sparse-CICPF is developed to achieve low-complexity detection of weak LFM astronomical signals with a long coherent integration time.

Note that, in the following discussion, lower and upper-case bold characters are used to denote vectors and matrices, respectively.

2. Signal Model

Consider a continuous-time signal consisting of weak astronomical chirp components, strong FH interferers, and additive complex white Gaussian noise. Let t_h denote the h-th system-wise hopping instant, at time instant $t \in [t_{h-1}, t_h)$, the received signal $s(t)$ can be expressed as

$$s(t) = \sum_{l=1}^{L} A_l e^{j\pi\left(2a_{l,1}t + a_{l,2}t^2\right)} + \sum_{k=1}^{K_h} A_{h,k} e^{j2\pi f_{h,k}t} + v(t), \qquad (1)$$

4

where A_l, $a_{l,1}$ and $a_{l,2}$ respectively denote the complex amplitude, initial frequency and chirp rate of the l-th astronomical components, and K_h represents the number of pure tones within the h-th system-wise dwell. In addition, $A_{h,k}$ and $f_{h,k}$ are the complex amplitude and carrier frequency of the k-th tone, respectively, and $v(t)$ denotes the additive complex Gaussian noise. Then, periodic sampling of $s(t)$ with the sampling interval of t_s yields the discrete-time received signal, expressed as

$$s[n] = \sum_{l=1}^{L} A_l e^{j\pi\left(2a_{l,1}nt_s + a_{l,2}(nt_s)^2\right)} + \sum_{k=1}^{K_h} A_{h,k} e^{j2\pi f_{h,k}nt_s} + v[n]. \qquad (2)$$

Consider a collection of N samples $\mathbf{x}[n] = [x[n-1], \ldots, x[n-N]]^{\mathrm{T}}$ as the observation data with $N - M$ missing samples, $0 < M \leq N$, and the positions of these missing samples are assumed to be randomly distributed. As such, $\mathbf{x}[n]$ can be regarded as the Hadamard product of the original data vector $\mathbf{s}[n] = [s[n-1], \ldots, s[n-N]]^{\mathrm{T}}$ and a binary mask vector $\mathbf{b}[n] = [b[n-1], \ldots, b[n-N]]^{\mathrm{T}}$, i.e.,

$$\mathbf{x}[n] = \mathbf{s}[n] \circ \mathbf{b}[n], \qquad (3)$$

with

$$b[n] = \begin{cases} 1, & \text{if } n \in \mathcal{J}, \\ 0, & \text{otherwise}, \end{cases} \qquad (4)$$

where $\mathcal{J} \subset \{1, 2, \ldots, N\}$ is the set of observed time instants with cardinality $|\mathcal{J}| = M$.

3. Sparsity-Based FH Signal Estimation and Suppression

The main steps of the proposed two-stage methodology are summarized in the flowchart depicted in Fig. 1. In this section, we provide a detailed explanation of the first step, i.e., sparsity-based FH signal estimation and mitigation, whereas the detection of weak astronomical signal is discussed in Section 4.

3.1. Joint-Variable Representations

The continuous-time definitions of the joint-variable representations can be found in [22]. Substituting $n \cdot t_s$ for the continuous-time index t, the
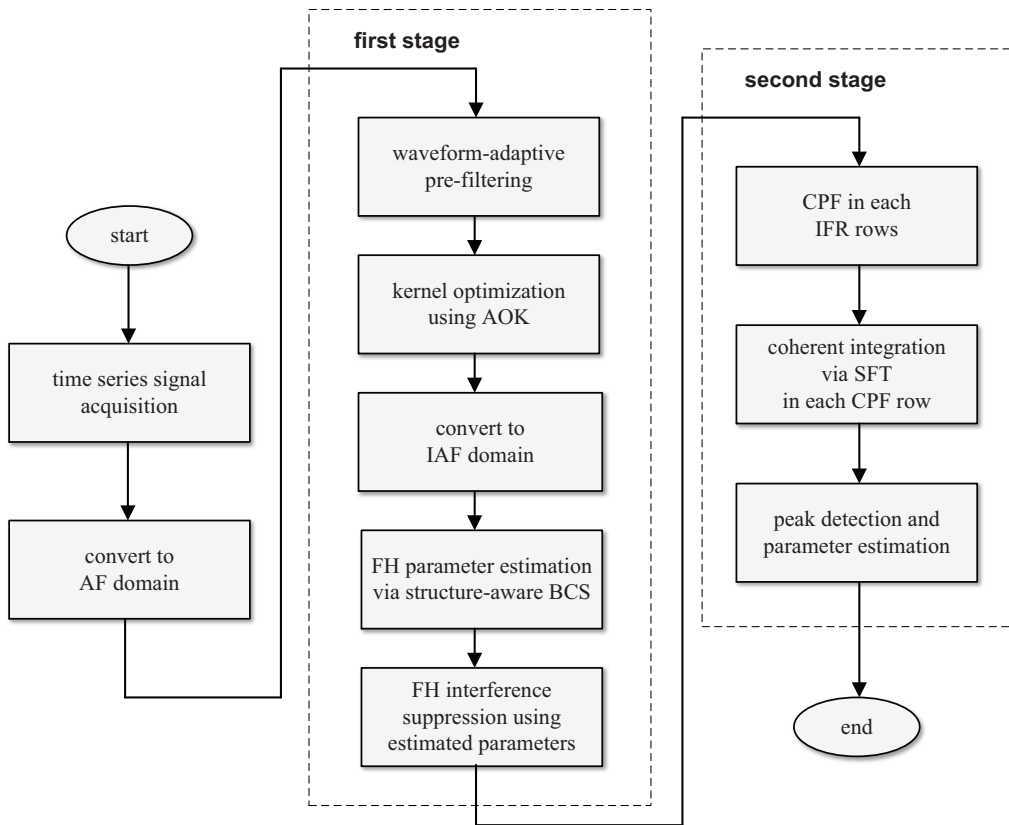
5

Figure 1: Flowchart of the proposed signal processing scheme.

discrete-time case can be established as follows. Let $\mathbf{C_{xx}}$ denote the instantaneous autocorrelation function (IAF) matrix, whose entry corresponding to time n and delay τ can be expressed as

$$C_{xx}[\tau, n] = x[n + \tau]x^*[n - \tau].\tag{5}$$

Then, the ambiguity function (AF) matrix of signal vector $\mathbf{x}[n]$, expressed w.r.t. time lag τ and Doppler frequency κ, can be obtained by performing IDFT of the IAF w.r.t. the time index n, i.e.,

$$\mathbf{A_{xx}}\{\tau, \kappa\} = \mathbf{F}_n^{-1}\mathbf{C_{xx}}\{\tau, n\} = \sum_n \mathbf{C_{xx}}\{\tau, n\}e^{\jmath 2\pi\kappa n},\tag{6}$$

where the notation $\{\tau, \kappa\}$ is used to emphasize that the matrix $\mathbf{A_{xx}}$ is constructed w.r.t. variables τ and κ. On the other hand, the Wigner-Ville dis-

tribution (WVD) can be obtained by performing DFT of the IAF w.r.t. the lag index τ, i.e.,

$$\mathbf{W_{xx}}\{f, n\} = \mathbf{F}_\tau \mathbf{C_{xx}}\{\tau, n\} = \sum_\tau \mathbf{C_{xx}}\{\tau, n\} \mathrm{e}^{-\jmath 4\pi f\tau}. \tag{7}$$

Note that, to make the discrete processing more convenient, there is a difference between the discrete-time IAF defined in (5) and the conventional definition of $C_{xx}[\tau, n] \triangleq x[n + \tau/2]x^*[n - \tau/2]$ in the sense that only integer lags are used in (5). This is a common practice in discrete-time bilinear time-frequency analysis (see, e.g., Chapter 6 of [22]). As a result, in (7), the exponential term $-\jmath 4\pi f\tau$ is used, rather than $-\jmath 2\pi f\tau$.

3.2. Waveform-Adaptive Kernel Design

Missing samples cause artifacts in the time-frequency domain [23], which must be mitigated before reliable FH interference parameter estimation can be performed. One of the techniques that achieves effective artifact mitigation is through the application of proper time-frequency kernels. A time-frequency kernel is a two-dimensional multiplicative low-pass filter in the AF domain, which can be translated to a two-dimensional convolution in the time-frequency domain. Time-frequency kernels can be either signal-independent or signal-dependent. As signal-dependent kernels perform parameter tuning adaptively, they generally provide better performance for artifact suppression and auto-term preservation. The AOK [24], which is based on radial Gaussian functions in the AF domain, is a commonly used signal-dependent kernel. With the optimization process in obtaining an AOK, the auto-term components are selected as much as possible within the low-pass Gaussian filter in the AF domain, while the pass-band area of the filter is limited to filter out the cross-terms which are located away from the AF origin.

However, the conventional AOK fails to filter out the near-origin artifacts induced by missing samples in the AF domain, which yields false vertical connections between multi-hopping-components in the resulting TFR. In the underlying problem, we can mitigate this problem by utilizing the *a priori* knowledge that the AF of the FH interference components is concentrated in the lag axis, whereas the AF of the missing-sample artifacts exhibits strong presence along the Doppler axis due to the impulsive nature of each missing sample. Thus, a proper pre-filtering window can be adopted before the kernel

7

optimization to prevent the artifacts from being falsely identified as desired signal components.

For signals with time-varying characteristics, the AOK is usually implemented with a time-localized short-time AF $A(t; \tau, \kappa)$ at each time instant t [24]. In our proposed method, prior to the radial kernel optimization procedure, the short-time AF is pre-filtered by utilizing a window, which is designed by thresholding the *a priori* knowledge-based conjectural single-component auto-term AF $\hat{A}[\tau, \kappa]$, expressed as [1]

$$\tilde{g}[\tau, \kappa] = \begin{cases} |\hat{A}[\tau, \kappa]|, & \text{if } |\hat{A}[\tau, \kappa]| > \xi, \\ 0, & \text{otherwise}, \end{cases} \tag{8}$$

where ξ is a threshold, which is chosen to only keep meaningful FH auto-terms in the AF domain. Then the pre-filtered short-time AF can be expressed as

$$\tilde{A}_{xx}(t; \tau, \kappa) = \tilde{g}[\tau, \kappa] \cdot A_{xx}(t; \tau, \kappa). \tag{9}$$

The TFR corresponding to the kernelled AF is obtained as its two-dimensional Fourier transform, expressed as

$$\tilde{\mathbf{W}}_{\mathbf{xx}}\{f, n\} = \mathbf{F}_{\tau, \kappa} \left[\tilde{\mathbf{A}}_{\mathbf{xx}}\{n; \tau, \kappa\} \circ \mathbf{\Phi}_{\text{opt}}\{n; \tau, \kappa\} \right], \tag{10}$$

where $\mathbf{\Phi}\{n; \tau, \kappa\}$ is the time-localized AOK matrix.

3.3. Structure-aware BCS-based FH Interference Mitigation

To suppress the FH interference, an accurate estimate of the FH parameters is required. Conventional Fourier-based TFRs do not generally provide a high-resolution signal energy representation. In this section, we consider a compressive sensing based approach which yields a high-resolution TFR. The compressive sensing approach obtains the kernelled TFR $\tilde{\mathbf{W}}_{\mathbf{xx}}\{f, n\}$ by exploiting the one-dimensional Fourier transform relationship in (7) but through a sparse reconstruction operation. Compared to the sparse TFR reconstruction based on the two-dimensional Fourier transform relationship between the AF and the TFR [25], those using the one-dimensional Fourier transform relationship between the IAF and the TFR yields improved performance with local sparsity constraints under lower computation complexity [26]. Denote the n-th column of the IAF matrix $\tilde{\mathbf{C}}_{\mathbf{xx}}\{\tau, n\}$ as $\tilde{\mathbf{c}}_{\mathbf{xx}}[n]$, and the n-th column of the bilinear TFR matrix $\tilde{\mathbf{W}}_{\mathbf{xx}}\{f, n\}$ as $\tilde{\mathbf{w}}_{\mathbf{xx}}[n]$. Then, their relationship conforms to the following standard linear model:

$$\tilde{\mathbf{c}}_{\mathbf{xx}}[n] = \mathbf{F}_f^{-1} \tilde{\mathbf{w}}_{\mathbf{xx}}[n]. \tag{11}$$

8

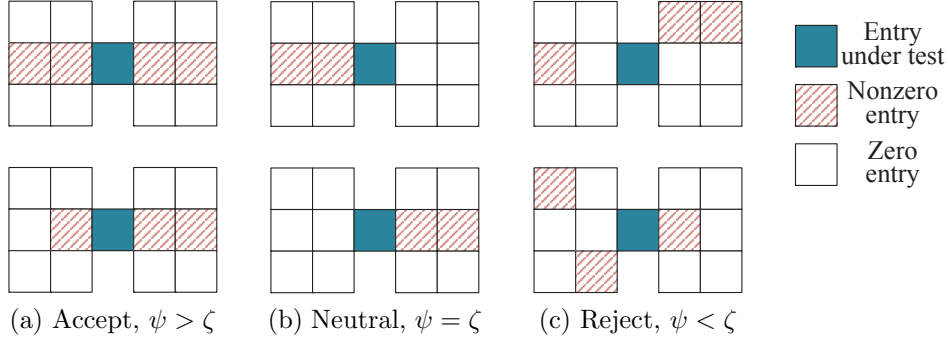(a) Accept, $\psi > \zeta$ (b) Neutral, $\psi = \zeta$ (c) Reject, $\psi < \zeta$

Figure 2: Example patterns of three different TFR categories.

Various compressive sensing algorithms can be used for sparse TFR reconstruction. In this paper, we use the structure-aware BCS method proposed in [2]. For notational convenience, we simplify the notations $\tilde{\mathbf{c}}_{\mathbf{xx}}[n]$, $\mathbf{F}_f^{-1}$ and $\tilde{\mathbf{w}}_{\mathbf{xx}}[n]$ as $\mathbf{c}$, $\boldsymbol{\Lambda}$ and $\mathbf{w}$, respectively. In this case, (11) is simplified as $\mathbf{c} = \boldsymbol{\Lambda}\mathbf{w}$.

The BCS is a nonparametric sparse linear inverse solver which assumes the likelihood model as [27]

$$p\left(\mathbf{c}; \mathbf{w}, \gamma_0\right) = \mathcal{CN}(\mathbf{c}; \boldsymbol{\Lambda}\mathbf{w}, \gamma_0\mathbf{I}), \tag{12}$$

where the variance γ_0 follows the inverse Gamma distribution, i.e., $\gamma_0^{-1} \sim$ Gamma(c, d). Note that, c, d here and a, b, ψ, ζ in the following discussion represent the model hyperparameters for the priors. To encourage sparsity of the FH signal TFR, a Dirichlet process prior with a spike-and-slab centering distribution [28, 29] is employed to the i-th entry of $\mathbf{w}$:

$$p(w_i; \gamma_i, \pi_i) = (1 - \pi_i)\delta_0 + \pi_i\mathcal{CN}(w_i; 0, \gamma_i), \tag{13}$$

where π_i is a mixing weight standing for the prior probability of a nonzero entry, δ_0 represents the delta function, and we also assign a Gamma prior to the precision as $\gamma_i^{-1} \sim$ Gamma(a, b). To make the inference analytical, a product of two latent variables z and θ, i.e., $w_i = z_i \cdot \theta_i$ is introduced to follow the PDF in (13), where $\theta_i \sim \mathcal{CN}(\theta_i; 0, \gamma_i)$, and z_i is a binary variable with $z_i \sim \mathcal{B}(\pi_i)$. $z_i = 1$ implies that the i-th entry is nonzero, whereas $z_i = 0$ implies a zero entry.

Because the FH spectrum shows a piecewise constant frequency spectrum, observed TFR patterns with such characteristics should be enhanced whereas TFR patterns deviating from such characteristics should be mitigated. Fig.

9

2 shows several TFR structure patterns for a neighborhood within an Euclidean distance of 2, where the horizonal direction shows the discretized time entries, and the vertical direction represents the frequency entries. The possible TFR structure patterns are divided into three categories, and different priors are designed to encourage the FH spectrum to have a horizontally linear structure. On the other hand, entries that are on adjacent rows are discouraged because they tend to broaden the signal bandwidth, thus are contradictory to the fact that the underlying FH signals are instantaneously narrowband.

Let set $\mathcal{J}_{\odot i}$ denote the neighborhood of index i, and $z_{\mathcal{J}_{\odot i}} = \sum_i z_i$ denote the total number of non-zero entries of z_i in this neighborhood. Then, by utilizing the conjugate property of the Beta and Bernoulli distributions, we analytically acquire the posterior distribution of π_i as

$$p\left(\pi_i; \psi, \zeta, z_{\mathcal{J}_{\odot i}}\right) = \text{Beta}\left(\psi + z_{\mathcal{J}_{\odot i}}, \zeta + |\mathcal{J}_{\odot i}| - z_{\mathcal{J}_{\odot i}}\right). \tag{14}$$

From (14) we can see that the amount of samples drawn for the mixing weight π_i in (13) is determined by $z_{\mathcal{J}_{\odot i}}$, ψ, and ζ. Therefore, the time-frequency structure pattern exerts impact on the prior by directly controlling the value of the $z_{\mathcal{J}_{\odot i}}$ term and the choice of the hyperparameters ψ and ζ.

The posterior probability is decided jointly by the likelihood and the prior. We adopt the maximum *a posteriori* (MAP) estimator to infer the estimation for $\mathbf{w}$ as

$$\hat{\mathbf{w}} = \arg\max_{\mathbf{w}} p\left(\mathbf{w} \,|\, \mathbf{c}\right), \tag{15}$$

where marginal distribution $p\left(\mathbf{w} \,|\, \mathbf{c}\right)$ can be obtained by integrating out the hyperparameters $\boldsymbol{\gamma}$, $\boldsymbol{\pi}$, and α_0 in the posterior distribution of $\mathbf{w}$ as

$$p\left(\mathbf{w} \,|\, \mathbf{c}\right) \propto \int p\left(\mathbf{w} \,|\, \boldsymbol{\gamma}, \boldsymbol{\pi}, \mathbf{c}, \alpha_0\right) \mathrm{d}\boldsymbol{\gamma}\mathrm{d}\boldsymbol{\pi}\mathrm{d}\alpha_0. \tag{16}$$

Hereby we obtain the sparse reconstruction result of (11). The estimation of the entire FH spectrum is rendered by repeating the BCS-based estimation for each column of $\tilde{\mathbf{W}}_{\mathbf{xx}}\{f, n\}$.

Once the interference IFs are estimated from sparse reconstruction as described above, we perform the signal stationarization that demodulates the IF of the selected signal to zero frequency, i.e., direct-current (DC) [30]. Then, the FH interference is suppressed through DC component removal, and the remaining signal is remodulated back [31]. To avoid performance degradation due to phase estimation error, we divide the entire data into multiple segments for separated processing.

4. Weak Astronomical Signal Detection

After FH interference removal, we will detect and estimate the weak LFM astronomical signals. We use the CICPF to make effective coherent integration of the LFM signals, where the SFT is used to achieve fast computations of the Fourier transform of the underlying sparse frequency modulated components. The CICPF is developed based on the cubic phase function (CPF), defined as [32]

$$P_{yy}[n, \Omega] = \sum_{\tau} y[n + \tau]y[n - \tau]e^{-\jmath\Omega\tau^2}, \tag{17}$$

where Ω denotes the instantaneous frequency rate (IFR), i.e., the second derivative of the signal phase w.r.t. the time index n. Stacking $P_{yy}[n, \Omega]$ corresponding to all values of n and Ω in a CPF matrix $\mathbf{P_{yy}}$, the weak auto-terms of the LFM astronomical signal can be enhanced by coherently integrating $\{f, \Omega\}$ energy along straight lines parallel to the time axis, i.e., [33]

$$\mathbf{P_{yy}}\{f, \Omega\} = \mathbf{F}_n\left(\mathbf{P_{yy}}\{n, \Omega\}e^{-\jmath\Omega n^2}\right). \tag{18}$$

For LFM signal components described in (2), the CICPF result will show spikes at location $(4\pi a_{l,1}t_s, 2\pi a_{l,2}t_s^2)$.
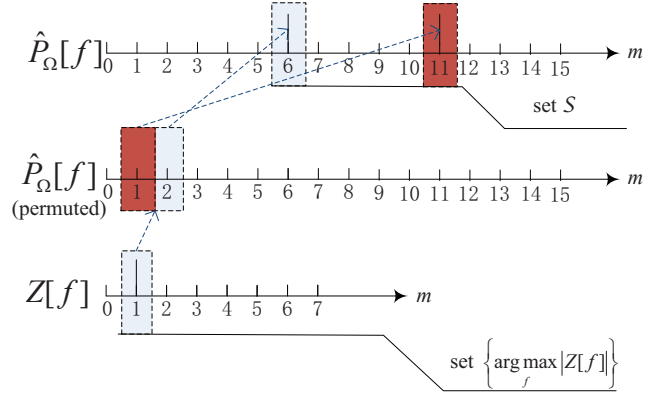
As the coherent integration of large-scale data using conventional fast Fourier transform is computationally demanding, we developed a sparse-CICPF based on SFT in this work. In this approach, the CPF in each IFR row is first dechirped with the corresponding value of Ω, and the resulting Ω-th row vector can be written as

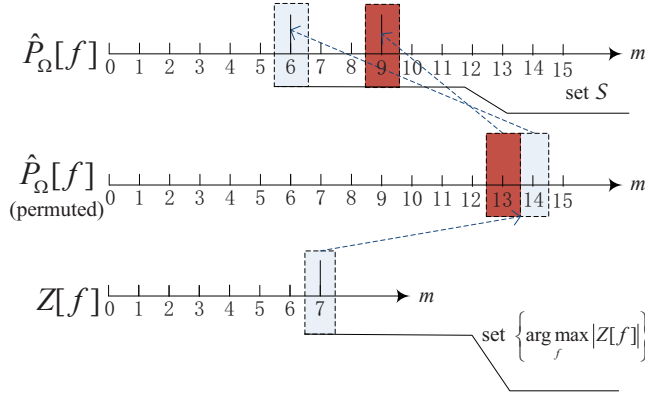$$\tilde{p}_{\Omega}[n] = \sum_{\tau} y[n + \tau]y[n - \tau]e^{-\jmath\Omega(\tau^2 + n^2)}. \tag{19}$$

The SFT is then applied to each row to obtain the CICPF in a similar manner as we proposed in [34]. To tear apart the nearby coefficients in the spectrum, a permutation is adopted to reorder the signals in the frequency domain as

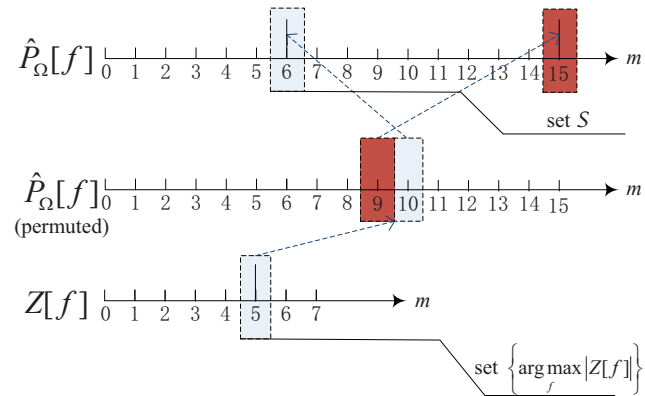$$z[n] = \tilde{w}[n] \cdot \tilde{p}_{\Omega}[[\sigma \cdot n] \bmod N], \quad n \in [1, N], \tag{20}$$

where $\sigma \in [1, N]$ is a random odd number that is invertible mod N, and σ^{-1} is a natural number such that $(\sigma \times \sigma^{-1}) \bmod N = 1$. Note that the permutated signal is filtered by a leakage-proof window $\tilde{w}[n]$. Let L_w denote

(a) $\sigma = 3$ $(\sigma^{-1} = 11)$

(b) $\sigma = 5$ $(\sigma^{-1} = 13)$

(c) $\sigma = 7$ $(\sigma^{-1} = 7)$

Figure 3: Illustrative examples of permutation with different values of σ. $(N = 16, B = 8)$

12

the window length in the time domain. We perform a reduced-dimensional fast Fourier transform (FFT) to a bucket consisting of B samples as

$$Z[f] = \text{FFT} \left\{ \sum_{i=0}^{\lfloor L_w/B \rfloor - 1} z[n + i \cdot B] \right\}, \quad n \in [1, B]. \tag{21}$$

The set of the coordinates of the estimated sparse component can be expressed as

$$\mathcal{S} = \left\{ f \in [1, N] \,\middle|\, h_\sigma[f] \in \left\{ \arg\max_f |Z[f]| \right\} \right\}, \tag{22}$$

where $h_\sigma(f)$ is a hash function defined as

$$h_\sigma[f] = \left\lfloor \frac{\sigma B}{N} \cdot f \right\rfloor. \tag{23}$$

Define an offset function

$$o_\sigma[f] = \sigma \cdot f - N \cdot h_\sigma[f]/B. \tag{24}$$

Then the estimated CICPF map becomes

$$\hat{P}_\Omega[f] = \begin{cases} \dfrac{Z[h_\sigma[f]]}{G[o_\sigma[f]]} \cdot e^{-j\pi o_\sigma[f] L_w/N}, & f \in \mathcal{S}, \\ 0, & f \notin \mathcal{S}. \end{cases} \tag{25}$$

We select a different value of σ and repeat (20)–(25) for an accurate estimation of the sparse spectrum at IFR Ω. To better explain the principle of the image to preimage mapping, which is the fundamental reason for the significant improvement of the efficiency in the proposed sparse-CICPF, three illustrative examples with different values of σ are shown in Fig. 3. The peaks corresponding to the true large coefficients remain stable in different σ loops, as such, the large-scale coherent integration process can be performed with reduced-dimensional operations.

5. Simulation Results

According to the IEEE 802.11 standard [35], at least 18 dB of the input SNR at the receiver end is needed for reliable communications. In the simulations, since the FH signal appears as interference, we set the SNR slightly

lower than the communication requirement but still strong enough for the weak signal detection. On the other hand, the astronomical signals usually have an SNR of -20 dB or less [36]. By adopting adaptive cancellation and spatial filtering techniques beforehand, the SNR can be improved. Therefore, we consider an example where the input SNR of the weak astronomical signal to be -16 dB, and the input interference-to-noise ratio (INR) of the FH interference to be 15 dB. The missing-sample rate of the signal data set is assumed to be 30%. The sampling rate is 15 MHz. A data set of length 2^{22} samples is considered in this paper. The astronomical signal consists of two components, whose initial frequencies are 324.4 MHz and 325.3 MHz, and chirp rates are -7.2 MHz/s and 21.6 MHz/s, respectively. The FH components from two interferers are randomly hopped within the $322.0-328.6$ MHz band that is shared by astronomy and tactical communications. To achieve a satisfactory performance and simultaneously keep the computational complexity within an affordable range, segmented processing is adopted. The segmentation length in the simulation is set to 256. The true spectrum of the FH interference in one segment is given in Fig. 4(a), where the solid black segments represent FH components.

Figs. 4(b) and 4(c) show the AF and WVD results without missing samples, while the missing-sample versions are presented in Figs. 4(d) and 4(e), respectively. The bilinear cross-terms can be observed in Figs. 4(d) and 4(e), along with the noise-like artifacts induced by the missing samples. Figs. 4(f) and 4(g) show the AF and TFR results using the proposed two-step kernel, where the cross-terms and artifacts are evidently mitigated. The results of the subsequent structure-aware BCS operation are presented in Fig. 4(h), which represent a significant improvement as compared to the WVDs depicted in Figs. 4(c) and 4(e). For comparison, we also present in Fig. 4(i) the result obtained by using the linear TFR based sparse Bayesian learning (SBL) approach in [11], which does not reveal a reliable FH spectrum. Based on the reconstructed spectrum in Fig. 4(h), the FH interference parameters can be accurately estimated. Fig. 4(j) shows the TFR after FH interference removal, which clearly confirms the effective removal of the FH interference. Note that the astronomical chirp signal remains invisible in this TFR plot because of its low SNR, and it cannot be revealed in the CPF processing either. To detect the weak astronomical signal, sparse CICPF is applied, and the result is shown in Fig. 4(k). Note that the IFR and the initial frequency are respectively normalized by $2\pi/N$ and 2π in the CPF and CICPF results. The locations of the two spikes on the CICPF plane are $(0.32, -0.1342)$ and
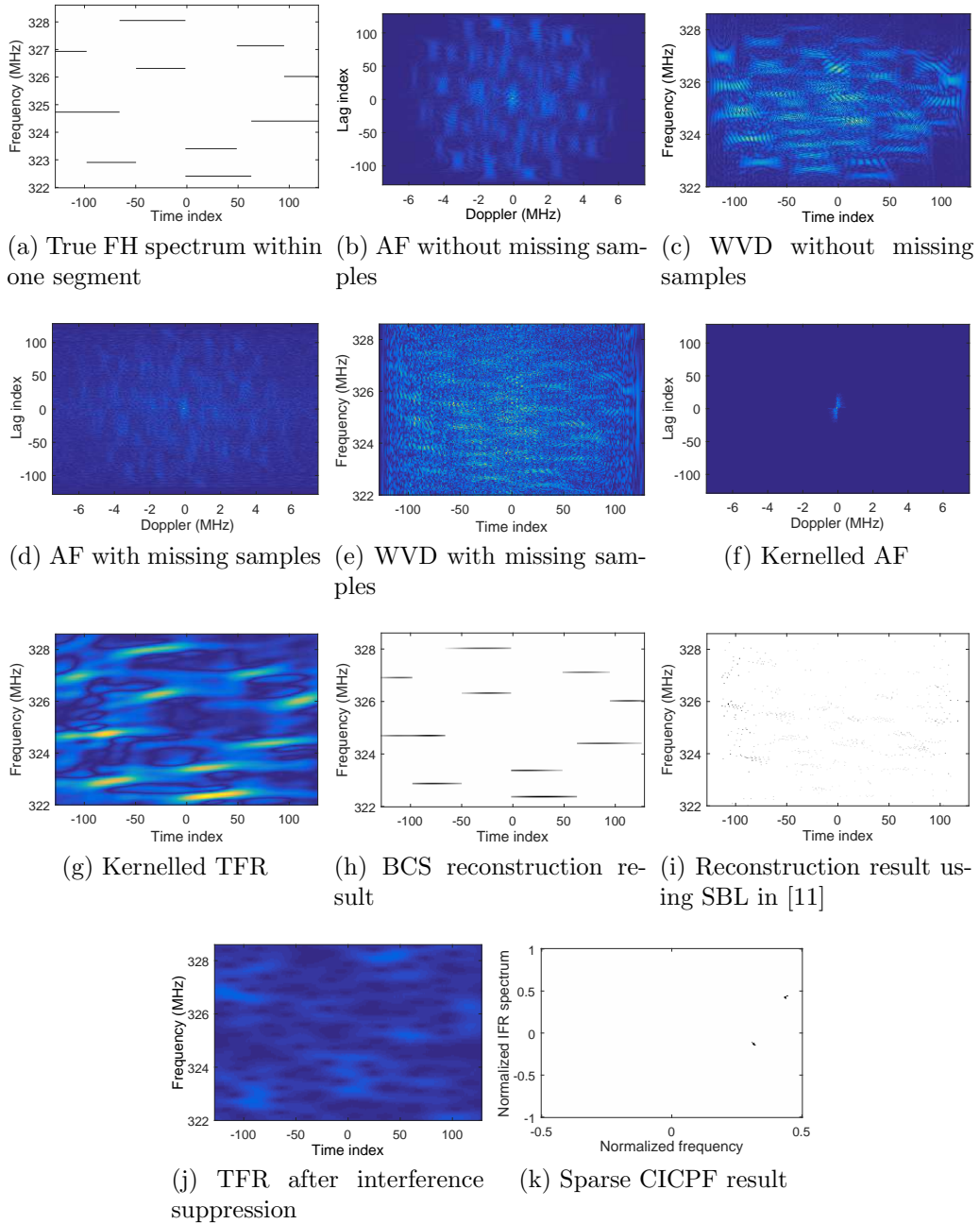
14

(a) True FH spectrum within one segment

(b) AF without missing samples

(c) WVD without missing samples

(d) AF with missing samples

(e) WVD with missing samples

(f) Kernelled AF

(g) Kernelled TFR

(h) BCS reconstruction result

(i) Reconstruction result using SBL in [11]

(j) TFR after interference suppression

(k) Sparse CICPF result

Figure 4: Simulation results.

15

$(0.44, 0.4027)$, respectively. From these results, the corresponding signal parameters can be accurately estimated. On the other hand, as we cannot effectively suppress the FH interference with the reconstruction result in Fig. 4(i), weak astronomical signal detection based on the method described in [11] is thus unrealistic.

Furthermore, we have run 1000 Monte Carlo trials to compare the performances of different approaches, where the input INR varies from 0 dB to 15 dB. Three different missing-sample ratios are also considered for the trials with the proposed scheme, and all the other parameter settings in the former simulation remain unchanged. Note that for the detection of the weak astronomical signals in the presence of strong FH interference, currently no existing method is reported in the literature. Therefore, in the Monte Carlo trials, we combine the state-of-the-art LFM signal detection algorithm CI-CPF [33] with the most recent FH parameter estimation techniques, i.e., sparse linear regression (SLR) [10], linear TFR based SBL [11], respectively, and take their results for comparison. When the input INR is low, the interference cannot be effectively suppressed while it is still much stronger than the desired weak astronomical signal, thus the detection probability is low. When missing samples exist, conventional linear TFR based methods fail to estimate the FH parameters, consequently weak astronomical signal cannot be detected in this case. Hence, the detection performance for the linear TFR based methods in the missing-sample case is not included in the figure. It can be concluded from Fig. 5 that the proposed scheme is superior to all the existing methods in terms of the detection performance, and the advantage is more remarkable in low INR regions. On the other hand, higher missing-sample ratios result in more severe decrease in the detection probability. However, the proposed scheme with 10% missing samples still performs slightly better than the SBL+CICPF scheme with no missing samples, and the proposed scheme with 20% missing samples remains advantageous to the SLR+CICPF scheme with no missing samples if the input INR is lower than 7 dB.

6. Conclusion

In this paper, we proposed a novel comprehensive scheme for robust astronomic signal reception in the presence of fast FH interference and missing data observations. The parameters of the FH interferers are estimated in the time-frequency domain through novel waveform-adaptive kernel design
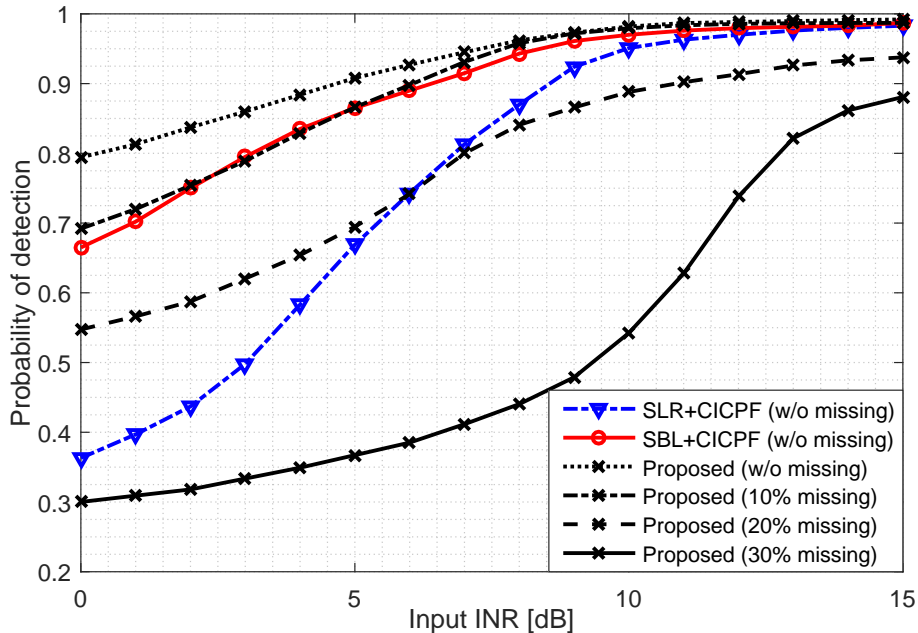
Figure 5: Statistic result through exhaustive Monte Carlo trials.

and structure-aware BCS-based sparse reconstruction. After FH interference suppression, the astronomical LFM signals are detected and accurately estimated using coherent signal integration based on the proposed sparse-CICPF approach. The presented method achieves robust and low-complexity adaptive parameter estimation of FH interference and weak astronomical signals in the presence of missing samples. The effectiveness of the proposed scheme is verified by simulation results. Future research efforts will focus on further performance improvement through, for example, the utulization of a continuous nonlinear function for optimal latent parameter determination with respect to the time-frequency neighboring patterns. We will also investigate the effect of gapped-missing samples in astronomy observation and the robust detection of astronomical signals in such challenging situations.

Acknowledgments

References

[1] S.-H. Liu, Y. D. Zhang, T. Shan, Sparsity-based frequency-hopping spectrum estimation with missing samples, in: Proc. 2016 IEEE Radar Conf., Philadelphia, PA, 2016, pp. 1–5.

[2] S.-H. Liu, Y. D. Zhang, T. Shan, S. Qin, M. G. Amin, Structure-aware Bayesian compressive sensing for frequency-hopping spectrum estimation, in: Proc. SPIE 9857, Compressive Sensing V: From Diverse Modalities to Big Data Analytics, Baltimore, MD, 2016, p. 98570N.

[3] P. J. Hall, The Square Kilometre Array: An Engineering Perspective, Springer, 2005.

[4] B. P. Abbott, R. Abbott, T. D. Abbott, et al., Observation of gravitational waves from a binary black hole merger, Phys. Rev. Lett. 116 (061102) (2016) 1–16.

[5] A. Leshem, A.-J. V. der Veen, Radio-astronomical imaging in the presence of strong radio interference, IEEE Trans. Inf. Theory 46 (5) (2000) 1730–1747.

[6] C. J. Law, G. Jones, D. C. Backer, W. C. Barott, G. C. Bower, C. Gutierrez-Kraybill, P. K. G. Williams, D. Werthimer, Millisecond imaging of radio transients with the pocket correlator, The Astrophysical Journal 742 (1) (2011) 1–12.

[7] J. Cohen, T. Spoelstra, R. Ambrosini, W. V. Driel, CRAF Handbook for Radio Astronomy, 3rd edition, Committee on Radio Astronomy Frequencies, European Science Foundation, 2005.

[8] Federal Government Spectrum Use Reports 225 MHz to 5 GHz, National Telecommunications and Information Administration (NTIA), 2014. Available at https://www.ntia.doc.gov/other-

publication/2014/federal-government-spectrum-use-reports-225-mhz-5-ghz_11142014.

[9] Radio Spectrum Use by the Radio Astronomy Service in Europe in the Frequency Band 29.7 to 960 MHz (CRAF-94-1), Committee on Radio Astronomy Frequencies, European Science Foundation, 1994. Available at http://www.craf.eu/documents/craf9401.doc.

[10] D. Angelosante, G. B. Giannakis, N. D. Sidiropoulos, Estimating multiple frequency-hopping signal parameters via sparse linear regression, IEEE Trans. Signal Process. 58 (10) (2010) 5044–5056.

[11] L. Zhao, L. Wang, G. Bi, L. Zhang, H. Zhang, Robust frequency-hopping spectrum estimation based on sparse Bayesian method, IEEE Trans. Wireless Commun. 14 (2) (2015) 781–793.

[12] M. Abed, A. Belouchrani, M. Cheriet, B. Boashash, Time-frequency distributions based on compact support kernels: Properties and performance evaluation, IEEE Trans. Signal Process. 60 (6) (2012) 2814–2827.

[13] B. Boashash, N. A. Khan, T. Ben-Jabeur, Time–frequency features for pattern recognition using high-resolution TFDs: A tutorial review, Digital Signal Process. 40 (2015) 1–30.

[14] F. Auger, P. Flandrin, Improving the readability of time-frequency and time-scale representations by the reassignment method, IEEE Trans. Signal Process. 43 (5) (1995) 1068–1089.

[15] F. Auger, P. Flandrin, Y.-T. Lin, S. McLaughlin, S. Meignen, T. Oberlin, H.-T. Wu, Time-frequency reassignment and synchrosqueezing: An overview, IEEE Signal Process. Mag. 30 (6) (2013) 32–41.

[16] I. Daubechies, J. Lu, H. Wu, Synchrosqueezed wavelet transforms: An empirical mode decomposition-like tool, Appl. Comput. Harmon. Anal. 30 (2) (2011) 243–261.

[17] S. Wang, X. Chen, Y. Wang, G. Cai, B. Ding, X. Zhang, Nonlinear squeezing time–frequency transform for weak signal detection, Signal Process. 113 (2015) 195–210.

[18] S. Meignen, D.-H. Pham, S. McLaughlin, On demodulation, ridge detection, and synchrosqueezing for multicomponent signals, IEEE Trans. Signal Process. 65 (8) (2017) 2093–2103.

[19] J. Gilles, Empirical wavelet transform, IEEE Trans. Signal Process. 61 (16) (2013) 3999–4010.

[20] J. P. Amezquita-Sanchez, H. Adeli, A new MUSIC-empirical wavelet transform methodology for time–frequency analysis of noisy nonlinear and non-stationary signals, Digital Signal Process. 45 (2015) 55–68.

[21] A. C. Gilbert, P. Indyk, M. Iwen, L. Schmidt, Recent developments in the sparse Fourier transform: A compressed Fourier transform for big data, IEEE Signal Process. Mag. 31 (5) (2014) 91–100.

[22] B. Boashash, Time-Frequency Signal Analysis And Processing: A Comprehensive Reference, 2nd Edition, Academic Press, 2015.

[23] Y. D. Zhang, M. G. Amin, B. Himed, Reduced interference time-frequency representations and sparse reconstruction of undersampled data, in: Proc. 21st Eur. Signal Process. Conf. (EUSIPCO 2013), Marrakech, Morocco, 2013, pp. 1–5.

[24] D. L. Jones, R. G. Baraniuk, An adaptive optimal-kernel time-frequency representation, IEEE Trans. Signal Process. 43 (10) (1995) 23612371.

[25] P. Flandrin, P. Borgnat, Time-frequency energy distributions meet compressed sensing, IEEE Trans. Signal Process. 58 (6) (2010) 2974–2982.

[26] M. G. Amin, B. Jokanovic, Y. D. Zhang, F. Ahmad, A sparsity-perspective to quadratic time-frequency distributions, Digital Signal Process. 46 (2015) 175–190.

[27] D. P. Wipf, B. D. Rao, Sparse Bayesian learning for basis selection, IEEE Trans. Signal Process. 52 (8) (2004) 2153–2164.

[28] L. Yu, J. P. Barbot, G. Zheng, H. Sun, Compressive Sensing for Cluster Structured Sparse Signals: Variational Bayes Approach, Technical Report, 2011. Available at http://hal.archives-ouvertes.fr/docs/00/57/39/53/PDF/clussvb.pdf.

[29] Q. Wu, Y. D. Zhang, M. G. Amin, Continuous structure based Bayesian compressive sensing for sparse reconstruction of time-frequency distributions, in: Proc. Int. Conf. Digital Signal Process., Hong Kong, China, 2014, pp. 831–836.

[30] Y. D. Zhang, M. G. Amin, B. Himed, Direction-of-arrival estimation of nonstationary signals exploiting signal characteristics, in: Proc. Int. Conf. Inf. Sci. Signal Process. Appl., Montreal, Canada, 2012, pp. 1223–1228.

[31] M. G. Amin, Y. D. Zhang, Nonstationary jammer excision for GPS receivers using sparse reconstruction techniques, in: Proc. ION GNSS+, Tampa, FL, 2014, pp. 3469–3474.

[32] P. Wang, J. Yang, Multicomponent chirp signals analysis using product cubic phase function, Digital Signal Process. 16 (6) (2006) 654–669.

[33] J. Su, H.-H. Tao, X. Rao, et al., Coherently integrated cubic phase function for multiple LFM signals analysis, Electron. Lett. 51 (5) (2015) 411–413.

[34] S.-H. Liu, T. Shan, R. Tao, Y. D. Zhang, G. Zhang, F. Zhang, Y. Wang, Sparse discrete fractional Fourier transform and its applications, IEEE Trans. Signal Process. 62 (24) (2014) 6582–6595.

[35] IEEE standard for information technology–telecommunications and information exchange between systems local and metropolitan area networks–specific requirements - part 11: Wireless LAN medium access control (MAC) and physical layer (PHY) specifications, IEEE Std. 802.11-2016.

[36] A.-J. van der Veen, A. Leshem, A.-J. Boonstra, Signal processing for radio astronomical arrays, in: Proc. IEEE Sens. Array Multichannel Signal Process. Workshop (SAM), Barcelona, Spain, 2004, pp. 1–10.